Ibn Al-Haitham Journal for Pure and Applied Sciences
Journal homepage: jih.uobaghdad.edu.iq
PISSN: 1609-4042, EISSN: 2521-3407
IHJPAS. 2024, 37(4)

The Effect of Annealing Process on Surface Plasmon Resonances in Tungsten Trioxide Films

Mohammed H. Mustafa[1,*] and Aliyah A. Shihab[2]
[1,2] Department of Physics, College of Education for Pure Sciences (Ibn Al-Haitham), University of Baghdad, Baghdad, Iraq.
*Corresponding Author

Received: 26 June 2023 Accepted: 1 August 2023 Published: 20 October 2024
doi.org/10.30526/37.4.3627

Abstract

In this study, after pyrolyzing the prepared solution, we made films from transitional tungsten oxide metal doped with gold nanoparticles and deposited them using a spray deposition technique on glass substrates at a substrate temperature of 320°C. We then annealed the prepared films at various temperatures (673,773 K) for one hour, in which we detected the band of localized surface plasmon resonance (LSPR) in gold-doped tungsten oxide films around the wavelength of 595 nm, and thermal treatment increased its intensity to near the wavelength of 580 nm. The produced and annealed thin films also demonstrated an indirect energy gap smaller than (2.86-2.61) eV in the UV-visible spectrum. The structural characteristics of the manufactured and annealed thin films reveal an amorphous structure at the substrate temperature of 320°C, but a polycrystalline structure at the annealing temperature, where researchers discovered monoclinic tungsten trioxide structures. (AFM), which achieved the maximum particle size of 75.93 nm after it was 47.85 nm, allowing researchers to see that the thin film of all the samples has a nanostructure.

Keywords: Structural, optical properties, surface plasmon resonances, WO_3 thin films.

1. Introduction

Due to their exceptional electrical characteristics, tungsten oxide films have recently attracted much scientific attention. Films can take various forms depending on the deposition conditions and methods [1-3]. The structural, optical, and electrical behaviors are very different. Additionally, there are other uses for these films, including electrocatalysis and gas sensors [4,5]. Various methods such as thermal evaporation, laser deposition, radio-frequency spattering, sol-gel, hydrothermal, spray pyrolysis, and others can create WO_3 thin films[6-8]. With a large band gap (E_g) of 2.5–3.2 eV, WO_3 has a monoclinic crystal structure [9-13]. This substance is exceptional for several reasons, including its low cost, chemical stability, non-toxicity, and mechanical properties. It is also thought to be a catalyst for semiconductors [14-17]. The current

study used spray pyrolysis to generate WO_3 thin films doped with gold nanoparticles. We periodically change the spray solution in the spray pyrolysis process to allow the adatoms enough time to break down. Avoid nozzle sprays because typical pyrolysis spray deposits frequently experience massive drop precipitation. The main purpose of this study is to investigate how annealing changes the crystal structure, optical properties, and surface properties of tungsten trioxide films created by spray pyrolysis.

2. 2. Methods and Material

This study used a molar concentration of 0.06 M and nano-gold doping to make tungsten trioxide thin films on glass substrates at 320°C. We used distilled water to dissolve H_2WO_4 powder, a source of tungsten oxide, in the presence of a small amount of ammonia. To create WO_3: Au films, dissolve them in water [18,19] and thoroughly agitate with a magnetic stirrer until the solution is clear. Then, add $HAuCl_4$, which represents the source of gold nanoparticles at a concentration of 6 mM, to the previously prepared solution. Using the pyrolysis spray approach, we deposited films with a thickness of 250 nm, spraying at a velocity of 0.15 ml/sec and maintaining 25 cm between the glass substrates and the spray nozzle. We anneal the prepared samples at temperatures of 673 K and 773 K. We examined the structural characteristics of all the prepared and annealed thin films using an (XRD). We examined the surface morphological properties of the film using atomic force spectrometry (AFM). We used a UV-Vis spectrophotometer with wavelengths between 300 and 1000 nm to examine the optical characteristics of the thin films.

3. Results and Discussion

3.1. Structural Analysis

3.1.1. XRD Analysis

Figure 1 illustrates the X-ray diffraction patterns of the WO_3 films without annealing and with annealing at different temperatures. at $2\Theta \sim 24^{o}$ in the film without annealing indicates an amorphous structure with short-range atomic organization in the crystal lattice. This feature might include dispersion from the glass and film substrates. According to the figure, tungsten trioxide exhibits an amorphous structure at 320 °C, and the peak at 2Θ=38.213° shows the cubic phase development of gold in (111) Orientation [20]. Using Scherrer's equation, the average crystal size of gold nanoparticles was calculated [21,22]. For the doped samples containing 6 mM of gold, the average size of the Au crystal was determined to be roughly 10.05 nm.

$$C.S = (0.94\ \lambda) / \beta \cos \Theta \quad (1)$$

Where:(λ) is the wavelength of XRD photons; is the full width at half maximum (FWHM); and (Θ) is the Brage diffraction angle in degrees.

After heating samples to 673K **Figure 1.** and **Table 1.**, we recognized reflections at the angles mentioned in **Table 1.** as the monoclinic WO_3 phase's reflections [13,23]. This film's recommended orientation is 200. According to **Figure 1.** and **Table 1.**, samples that were annealed

at 773 K likewise showed evidence of the WO_3 phase, but with a preferred orientation of (002). Based on CAS Number (1314-35-8), peak position and plane indices are also displayed.

Table 1. Peak positions (2Θ), spacing (d), planes (hkl), and crystallite size (C.S), of WO_3:Au as-deposited films and annealed at 673 K and 773 K.

Ta (k)	2θ(deg.) Exp.	d (Å) ASTM	d (Å) Exp.	Phase	Planes (hkl)	C.S (nm)
673	23.202	3.8440	3.8428	Mon. WO_3	(002)	18.1206
	23.619	3.7690	3.7673	Mon. WO_3	(020)	14.5837
	24.419	3.6480	3.6469	Mon. WO_3	(200)	16.5344
	38.208	2.3550	2.3547	Cub. Au	(111)	10.6557
	44.337	2.0390	2.0383	Cub. Au	(200)	9.06666
773	23.179	3.8440	3.8433	Mon. WO_3	(002)	18.8330
	23.597	3.7679	3.7690	Mon. WO_3	(020)	15.8988
	24.399	3.6480	3.6474	Mon. WO_3	(200)	17.4157
	34.172	2.6230	2.6223	Mon. WO_3	(209)	14.4891
	38.198	2.3550	2.3550	Cub. Au	(111)	11.3229
	44.363	2.0390	2.0395	Cub. Au	(200)	12.5702

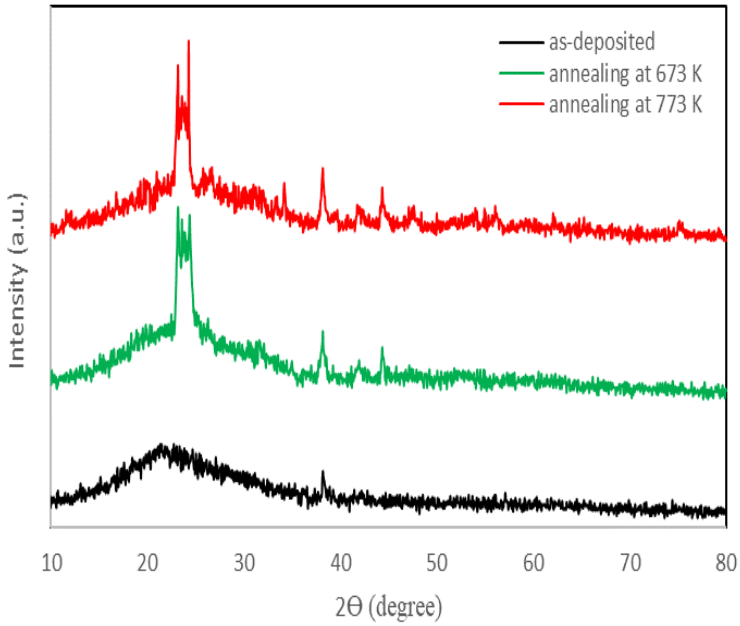

Figure 1. X-ray diffraction pattern of WO_3: Au films without annealing and with annealing at different temperatures.

3.1.2. The Surface Morphology Analysis

Figure 2. displays the AFM pictures of the deposited and annealed WO_3 thin films. The films' surfaces are smooth and have grains between (47 and 76) nm in size. The deposited films did not clearly show the grain boundaries, but annealing made them more obvious.

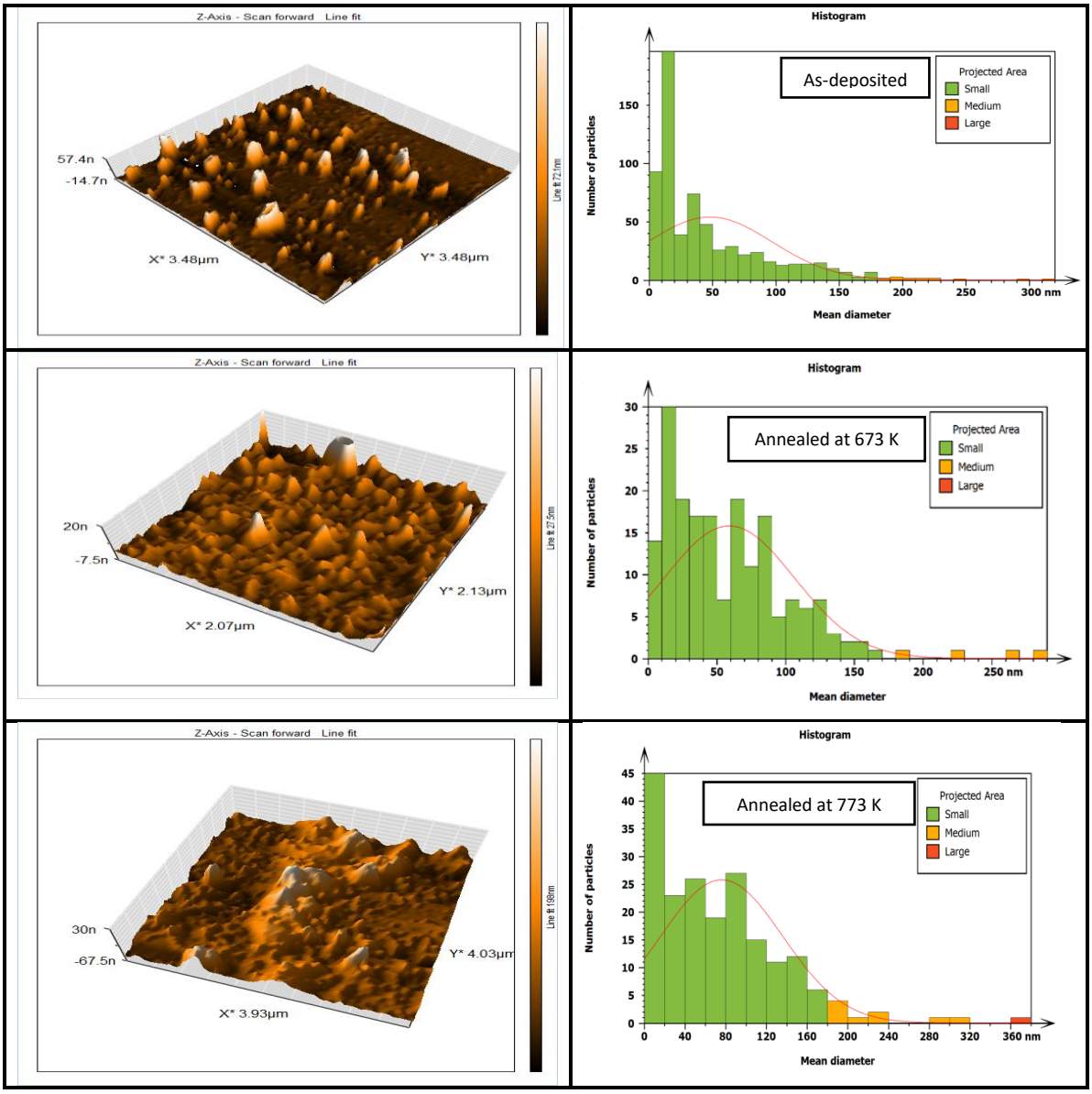

Figure 2. AFM images of WO_3: Au thin films without annealing and with annealing.

The films' particle sizes grow as the annealing temperature rises. We discovered that the RMS value changed, and the surface remained smooth continuously. Surface roughness increases only slightly because of annealing. Some deep valleys developed, and the structure became more distinct. Films produced and annealed at 673 K and 773 K have smooth surfaces and contain nanoscale particles.

Table 2. displays the roughness and typical grain size of synthetic and annealed films. According to **Figure 2.**, the films' grain size increased as the annealing temperature rose. High temperatures caused the grains to grow and become clearer. The surface's continuous structure changed into a distinct one.

Table 2. The roughness and average grain size thin films of WO_3:Au as-deposited sample and when annealed at two temperatures 673 K and 773 K.

Annealing Temperature (K)	Average diameter (nm)	Roughness Average (nm)	Root mean square (nm)
As-deposited	47.85	11.71	16.39
673	59.01	40.58	51.59
773	75.93	56.38	69.85

3.2. Optical Analysis

The optical transmittance plots of the WO_3 films are displayed in **Figure 3**. All films exhibit high visible-range transmittance, which denotes a low level of oxygen ion vacancies [24,25]. Below $\lambda = 400$ nm, the transmittance values decrease dramatically, indicating significant band-to-band absorption [26]. The total transmittance of the films was not considerably altered by raising the annealing temperature, it caused the absorption edges to move to lower energy ranges, resulting in a reduction in band gaps.

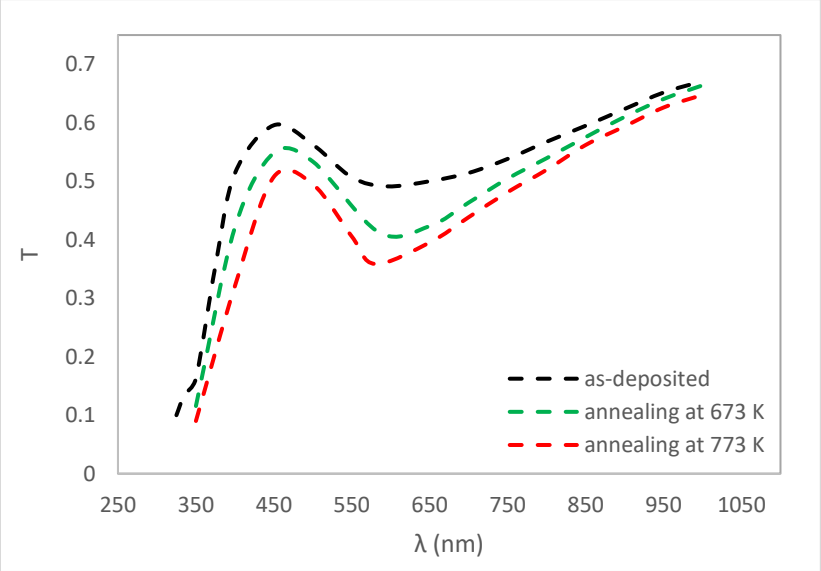

Figure 3. The transmission spectrum for WO_3:Au films as a function of wavelength.

The band gap values of WO_3 doped with gold nanoparticles and annealed with different temperature films can be obtained by extrapolating the straight-line section of the $(\alpha h\upsilon)^{1/2}$ versus $(h\upsilon)$. **Figure 4.** and **Table 3.** show that after the annealing process, the energy gap for tungsten oxide films doped with gold nanoparticles dropped from 2.86 eV to 2.61 eV. The films' decreased oxygen content due to their annealing at high temperatures is thought to be the drop in the value of E_g^{opt}. This conclusion is in line with [13, 23, 27, 28].

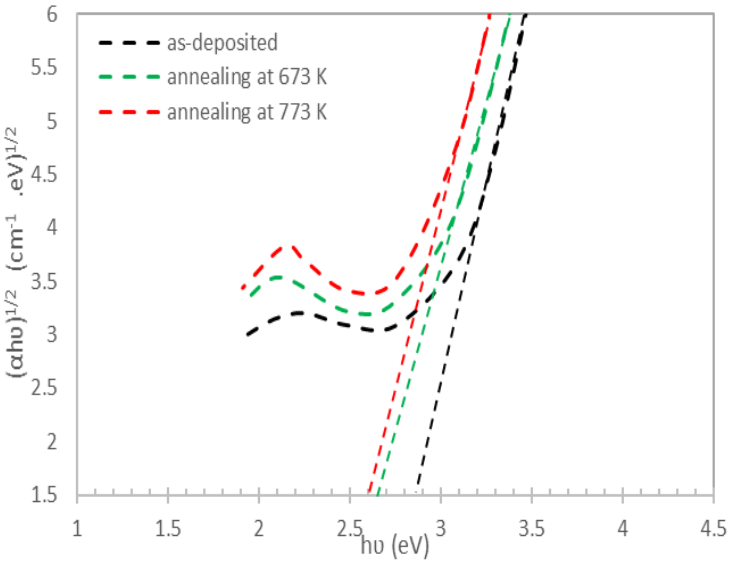

Figure 4. The plot of $(\alpha h\upsilon)^{1/2}$ as a function of $(h\upsilon)$ for WO_3:Au thin films.

Table 3 displays data from various WO_3 probes, including Au at full width at half maximum (FWHM) and LSPR peak position (SPR). The transmittance spectra of the gold-embedded film show a reduction at about 595 nm, possibly due to absorption from gold nanoparticles' surface plasmon resonance (SPR). The main reason why the LSPR absorption band gets stronger with temperature is that Au nanoparticles get bigger [29, 30]. According to figure 3, as the annealing temperature changes, the position of the LSPR peak also shifts, with the orange hue reverting to yellow at the 773 K LSPR at 580 nm after moving away from the SPRAD at 595 nm. This behavior is comparable to that seen by the researcher [3] after annealing doped tungsten oxide films to various annealing intensities.

Table 3. Energy gap (E_g), full width at half maximum (FWHM), and LSPR peak location (λ_{SPR}) for WO_3:Au as-deposited and at the different annealing temperatures.

Annealing temperature (K)	E_g (eV)	FWHM (nm)	λ_{SPR} (nm)
As deposited	2.86	327	595
673	2.67	255	585
773	2.61	236	580

4. Conclusion

Electron beam evaporation deposited WO_3:Au sheets with a thickness of 250 nm on glass substrates. We demonstrate both the amorphous WO_3:Au films and the crystalline films produced following the annealing temperature have surfaces with homogeneous shapes and no surface cracks. The annealing temperature promotes the formation of thin films with a nanocrystalline structure. The energy band gap is 2.86 eV before annealing and 2.67 eV and 2.61 eV after annealing respectively.

Acknowledgment

I would like to thank the staff of the Physics Department, Deanship of the College of Education for Pure Science (Ibn Al-Haitham) for their support in writing this research.

Conflict of Interest

The authors declare that they have no conflicts of interest.

Funding

None.

References

1. Kadam, P.M. Enhanced optical modulation due to SPR in gold nanoparticles embedded WO_3 thin films. *Journal of Alloys and Compounds* **2011**, *509(5)*, 1729–1733. https://doi:10.1016/j.jallcom.2010.10.024
2. Charles, C.; Martin, N.; Devel, M.; Ollitrault, J. Correlation between structural and optical properties of WO_3 thin films sputter deposited by glancing angle deposition. *Thin Solid Films* **2013,** *534*, 275–281. https://doi.org/10.1016/j.tsf.2013.03.004
3. Figueiredo, N.M.; Vaz, F.; Cunha, L.; Cavaleiro, A. Au-WO_3 nanocomposite coatings for localized surface plasmon resonance sensing. *Materials* **2020,** *13(1)*, 246-450. https://doi:10.3390/ma13010246
4. Keshri, S.; Kumar, A.; Kabiraj, D. Effect of Annealing on Structural, Optical and Electrical Behaviors of WO_3 Thin Films Prepared by Physical Vapour Deposition Method. *Journal of Nano-and Electronic Physics* **2011,** *3(1)*, 260-266.
5. Hutchins, M.G.; Abu-Alkhair, O.; El-Nahass, M.M.; Abdel-Hady, K. Electrical conduction mechanisms in thermally evaporated tungsten trioxide (WO_3) thin films. *Journal of Physics: Condensed Matter* **2006,** *18(44)*, 9987. https://doi:10.1088/0953-8984/18/44/401
6. Mohammed, F.A.; Salim, E.T.; Hassan, A.I.; Wahid, M.H. Effect of precursor concentration on the structural, optical, and electrical properties of WO_3 thin films prepared by spray pyrolysis. *Journal of Applied Sciences and Nanotechnology* **2022,** *2(4)*, 91–105. https://doi:10. 53293/jasn.2022.4715.1139
7. Shuihab, A.; Khalf, S. Fabrication and characterization of nickel oxide nanoparticles /silicon NiO NPS/Si. *in AIP Conference Proceedings, AIP Publishing* **2018,** *11*, 2224. https://doi.org/10.1063/1.5039185
8. Ali, L.S.; Shehab, A.A.; Abd, A.N. Preparation and characterization of p-NiO: Li thin films as Schottky photodiode. *in Journal of Physics: Conference Series, IOP Publishing* **2019,** *22*, 012050. https://doi:10.1088/1742-6596/1234/1/012050
9. Madhukar, P.; Jayababu, N.; Ramana, R.; Shanmukhi, J. Study of structural, morphological and electrical properties of WO_3 thin films by e-beam technique. *Journal of Pure Applied and Industrial Physics* **2017,** *7(11)*, 405–413. https://doi:10.29055/128/jpaip/2934
10. Feng Y. Fabrication of WO_3 photoanode on crystalline Si solar cell for water splitting. *J Mater Sci: Mater Electron* **2020,** *31(17)*, 14137–14144, https://doi:10.1007/s10854-020-03968-6
11. Bertus, L.M.; Enesca, A.; Duta, A. Influence of spray pyrolysis deposition parameters on the optoelectronic properties of WO_3 thin films. *Thin Solid Films* **2012,** *520(13)*, 4282–4290. https://doi:10.1016/j.tsf.2012.02.052
12. De León, J.R.; Acosta, D.R.; Pal, U.; Castaneda, L. Improving electrochromic behavior of spray pyrolised WO_3 thin solid films by Mo doping. *Electrochimica Acta* **2011,** *56(5)*, 2599–2605. https://doi:10.1016/j.electacta.2010.11.038
13. Simchi, H.; McCandless, B.E.; Meng, T.; Shafarman, W.N. Structural, optical, and surface properties of WO_3 thin films for solar cells. *Journal of Alloys and Compounds* **2014,** *617*, 609–615, https://doi:10.1016/j.jallcom.2014.08.047

14. Gullapalli, S.K.; Vemuri, R.S.; Ramana, C.V. Structural transformation induced changes in the optical properties of nanocrystalline tungsten oxide thin films. *Applied Physics Letters* **2010,** 96*(17),* 11-24. https://doi:10.1063/1.3421230
15. Bertus L.M. Synthesis and characterization of WO_3 thin films by surfactant-assisted spray pyrolysis for electrochromic applications. *Materials chemistry and physics* **2013,** *140(1),* 49–59. http://doi.org/10.1016/j.matchemphys.2013.02.047
16. Amri A. Surface structural features and optical analysis of nanostructured Cu-oxide thin film coatings coated via the sol-gel dip coating method, *Ceramics International* **2019,** *45(10),* 12888–12894, https://doi:10.1016/j.ceramint.2019.03.213
17. Salim, E.T.; Hassan, A.I.; Mohamed, F.A.; Wahid, M.H.; Fakhri, M.A. A sight of view on electrical impacts, structural properties and surface roughness of tungsten trioxide thin film: effect of substrate temperatures in WO_3/Si device fabrication. *Physica Scripta*. **2023,** *98(3),* 035508, https://doi:10.1088/1402-4896/acb8ea
18. Arifuzzaman, M. Investigation of silver doping on structural, optical and electrical properties of spray deposited tungsten trioxide thin films. **2021,** *11,* 213. http://doi:8080/xmlui/handle /123456789/5967
19. Mustafa M.H.; Shihab, A.A. Influence of heat treatment on the efficiency of WO_3: Au NPs optoelectronic device prepared by spray pyrolysis technique. *Journal of Theoretical and Applied Physics (JTAP)* **2024,** *11*, 224. https://doi:10.57647/j.jtap.2024.si-AICIS23.07
20. Naseri, N.; Azimirad, R.; Akhavan, O.; Moshfegh, A.Z. Improved electrochromic properties of sol-gel WO_3 thin films by doping gold nanocrystals. *Thin Solid Films* **2010,** *518(8),* 2250–2257. https://DOI:10.1016/j.tsf.2009.08.001
21. Mustafa, M.H.; Shihab, A.A. Effect of ratio gold nanoparticles on the properties and efficiency photovoltaic of thin films of amorphous tungsten trioxide. *Journal of Ovonic Research* **2023,** *19(6),* 23-34. https://DOI:10.15251/JOR.2023.196.623
22. Gregory, N.W. Elements of X-Ray Diffraction. *J. Am. Chem. Soc.* **1957,** *79(7),* 1773–1774. https://doi:10.1021/ja01564a077
23. Yousif A.; Khudadad, A.I. Effects of annealing process on the WO_3 thin films prepared by pulsed laser deposition. *in IOP Conference Series: Materials Science and Engineering*, *IOP Publishing* **2020,** *11*, 012064. https://doi:10.1088/1757-899X/745/1/012064
24. Xu, C. Effect of oxygen vacancy on the band gap and nanosecond laser-induced damage threshold of Ta_2O_5 films. *Chinese Physics Letters* **2012.** *29(8),* 084207, https://doi.org/10.1088/0256-307X/29/8/084207
25. Sabhapathi V.K. Optical absorption studies in molybdenum trioxide thin films. *Phys. Stat. Sol. (a)* **1995,** *148(1),*167–173. https://doi:10.1007/BF02745144
26. Pankove, J.I. Optical processes in semiconductors. *Courier Corporation* **1975,** *23*, 341-348.
27. Joraid A.; Alamri, S.N. Effect of annealing on structural and optical properties of WO_3 thin films prepared by electron-beam coating. *Physica B: Condensed Matter* **2007,** *391(2),* 199–205. https://DOI:10.1016/j.physb.2006.09.010
28. Saeed, M.H.; Al-Timimi, M.H.; Hussein, O.A. Structural, morphological and optical characterization of nanocrystalline WO_3 thin films. *Digest Journal of Nanomaterials and Biostructures* **2021,** *16(2),* 563–569, https://doi:10.15251/DJNB.2021.162.563
29. Louis C.; Pluchery, O. *Gold Nanoparticles for Physics, Chemistry and Biology (Second Edition)* **2017,** *12*, 23-35.
30. Kreibig U.; Vollmer, M. Optical properties of metal clusters. *Springer Science & Business Media* **2013,** *25*, 224-234.